Surface & Coatings Technology 482 (2024) 130631

Contents lists available at ScienceDirect

Surface & Coatings Technology

journal homepage: www.elsevier.com/locate/surfcoat

Full Length Article

Corrosion and antifouling properties of copper-containing PEO coatings produced on steels

Luca Pezzato [a,*], Sajjad Akbarzadeh [b], Alessio Giorgio Settimi [a], Emanuela Moschin [c], Isabella Moro [c], Marie-Georges Olivier [b], Katya Brunelli [a], Manuele Dabalà [a]

[a] Department of Industrial Engineering, University of Padova, Via Marzolo 9, 35131 Padova, Italy
[b] Materials Science Department, Faculty of Engineering, University of Mons, 20 Place du Parc, 7000 Mons, Belgium
[c] Department of Biology, University of Padua, Via Ugo Bassi 58/B, 35131, Padova, Italy

ARTICLE INFO

Keywords:
Plasma electrolytic oxidation
Coating
Copper
Antifouling
SVET
EIS

ABSTRACT

In this work, antifouling copper-containing PEO coatings were produced on zinc-aluminized steels and their antifouling properties in circulating seawater were tested at the Hydrobiological Station Umberto D'Ancona located in Chioggia (Venice, Italy). The effect of the presence of the copper particles on the localized corrosion properties of the PEO coatings was also investigated in depth. In detail, the PEO-coated samples were produced and characterized in terms of microstructure and phase composition through SEM and XRD analysis. The antifouling properties of the samples were evaluated through stereo-microscope and SEM observations after up to 28 days of immersion and the corrosion properties were analyzed with EIS and SVET tests. The results, besides the successful incorporation of the copper particles into the coatings, evidenced the remarkable antifouling effect of the copper particles which also produced a clear selection in the type of algae that can colonize the samples. Considering the corrosion properties, the copper particles were found to be detrimental, due to the galvanic coupling with the substrate. Considering both results, the copper-containing PEO coating can be suggested only in combination with a topcoat which further increases the corrosion performance.

1. Introduction

The PEO (Plasma Electrolytic Oxidation) process is a promising coating technique characterized by a large number of potential applications which span the aerospace, naval, construction, electrical, biomedical, oil/gas processing, textile, sports, and leisure sectors of industry [1,2]. The large number of possible technological applications is related to the characteristics of the hard oxide coating formed over the metal surface, and, in particular, the high hardness, the very high corrosion [3] and wear resistance [4], the possibility to incorporate compounds from the electrolyte into the coating [5–7], the possibility to use the coating as pre-treatment for different top coatings [8], the biocompatibility [9] and the thermal barrier effect of the coating [10].

A large part of the works present in the literature on the applications of the PEO process deal with light alloys, such as aluminum, titanium, and magnesium alloys, which are often employed as substrates for the process [7,11,12]. PEO process was also applied with success to other particular alloys such as Zinc alloys [13], Niobium alloys [14] and Zirconium alloys [15]. Several attempts have been made to obtain PEO coatings on steels [16–18] but up to now, coatings with acceptable performances have been obtained only on pre-aluminized steels [19]. One of the more novel approaches in this sense was proposed by the authors with the successful use of zinc-aluminized steels as a substrate for PEO coatings [20], thus permitting a protective oxide film to also be formed on steel, which remains the most widely employed material for industrial and civil applications.

The characteristics of the coating strongly depend on the process parameters employed during the PEO process, and, in particular, the electrical parameters [21]. The literature agrees on the fact that the best coatings in terms of density, wear, and corrosion properties can be obtained with pulsed current (PC) mode in comparison to direct current (DC) mode [22,23]. This fact is linked to the mechanism of formation of the coating and, in particular, with the more "soft" and controlled discharge phenomena in PC mode [24,25].

The versatility of the process is mainly related to the fact that, due to the discharge phenomena that occur during the formation of the coating,

* Corresponding author at: Department of Industrial Engineering, University of Padova, Via Marzolo 9, 35131 Padova, Italy.
E-mail address: luca.pezzato@unipd.it (L. Pezzato).

https://doi.org/10.1016/j.surfcoat.2024.130631
Received 25 November 2023; Received in revised form 14 February 2024; Accepted 6 March 2024
Available online 15 March 2024

it is possible to functionalize the surface by simply adding compounds into the electrolyte [26]. These compounds, in fact, can enter into the discharge channels formed during the process and subsequently be inertly incorporated into the coating or react with other chemical species permitting the formation of a coating with unique compositional properties [27]. The functionality given to the surface is strongly linked to the type of additive added into the electrolyte, and can range from the improvement of the corrosion or wear properties [28], to optical properties [29], moving towards the realization of surfaces with antibacterial or antifouling activity [30]. This last possibility has already been studied by the authors on aluminum alloys [31] and preliminary on steels [32] with the addition of copper particles into the coating in order to confer an antifouling effect.

The antifouling effect of copper is well known both in the literature and in the industrial world [33], and, as a matter of fact, the majority of tin-free antifouling paints currently available contain copper [34]. The exploitation of the antifouling effect occurs due to the release of copper ions that are able to kill biological cells [35]. Copper is, however, a metal characterized by a significantly different potential in comparison to steels in the nobility scale of the metals, and this can cause galvanic corrosion when the two metals are in contact [36].

This work aims to study the antifouling effect of copper particles incorporated into PEO coatings produced on zinc-aluminized steels in depth and to analyze their effect on the corrosion properties of the substrate. The antifouling properties were, in fact, already preliminarily evaluated by the authors in a previous work, but in this work there is a more in depth investigation of the type of algae that are involved in the fouling process and the influence of the type of substrate on the type of colonization. Moreover, the corrosion mechanism was studied more intensely with specific localized corrosion tests (SVET tests) that permitted the specific study of the effect of the incorporated particles on the corrosion properties of the coatings. Copper-containing PEO coatings were found to possess strong antifouling properties, especially during the first weeks of immersion, also producing remarkable changes in algal biodiversity which create eventual colonization in comparison with the PEO and Untreated samples. Moreover, the influence of the copper particles on the corrosion properties of the PEO-coated samples was investigated in depth in terms of localized corrosion performances evidencing a negative effect of the particles on the corrosion properties of the substrate.

2. Materials and methods

Commercial Galvalume coated carbon steel samples (55 % Al, 45 % Zn) were used as substrates for PEO coatings. In detail were employed sheets with dimensions 3 × 1 cm. Before the treatment, the samples were degreased by an ultrasonic bath in acetone for 10 min. The employed electrolyte consists of an aqueous solution of 25 g / l L of Na_2SiO_3 and 2.5 g / l L of NaOH with the addition of 15 g / l L of metallic copper particles with an average size of approximately 0.45 μm. The electrolyte and the quantity of copper particles were decided based on the previous work of the authors [32] and on the basis of the chemical stability of the electrolyte, considering the fact that an excessive amount of copper particles resulted in a precipitation of the copper. During the treatment, the bath was continuously stirred in order to maintain the particles in suspension.

A TDK-Lambda Direct Current power supply (500 V/8 A) was used for the PEO treatment in which the sample worked as an anode while the cathode was made up of a carbon steel cage. The treatments were performed keeping the current density constant and letting the potential free to vary working in unipolar pulsed Current mode: 0.75 A / cm^2 in the pulsed current (with a frequency of 200 Hz and a duty cycle of 50 %). The pulsed effect of the current was obtained with a customized system of switches. In order to understand the effect of the presence of the copper particles on the corrosion and antifouling properties, samples were produced with and without the addition of copper. In all the cases the treatment time was 120 s.

After treatment, the samples were washed with deionized water and ethanol and dried with compressed air. The cross-sections of the treated samples were cut and mounted in epoxy resin, then polished with a standard metallographic technique (grinding with SiC abrasive papers from 500 to 1200 grit and polishing with cloths with 6- and 1-μm diamond suspensions). Both the surfaces and the cross sections were analyzed with a scanning electron microscope (SEM) Cambridge Stereoscan LEO 440, equipped with Philips PV9800 EDS microanalysis, in order to evaluate the morphological characteristics, the thickness of the coating and the elemental composition, as well as the clear presence, or not, of the particles. The phase composition was evaluated by X-ray diffraction analysis (XRD) using a Siemens D500 diffractometer (Siemens, Munich, Germany) using Cu-Kα radiation (step size 0.05°, counting time 5 s).

The corrosion properties of the various samples were evaluated with electrochemical impedance spectroscopy (EIS) tests at room temperature. EIS tests were performed in a solution containing 0.1 M Na_2SO_4 and 0.05 M NaCl, in order to simulate a moderate aggressive environment, with an AMEL 2549 Potentiostat, using a saturated calomel electrode as the reference electrode (SCE) and a platinum electrode as the counter electrode. The tests were done at the value of the open circuit potential (OCP) and in a frequency range between 10^5 Hz and 10^{-2} Hz with a perturbation amplitude of 10 mV. The impedance measurements were recorded with a Materials Instrument Spectrometer coupled with the 2549 Potentiostat, and the *Z*-View software (version 3.3) was used for the fitting of impedance spectra. EIS tests were performed using an exposed area of 1 cm^2 and after 30 min of OCP stabilization. All the tests were repeated three times to ensure reproducibility.

Localized corrosion properties were further evaluated by Scanning Vibrating Electrode Technique (SVET) in 15 mM NaCl electrolyte. The cut-edge configuration of the panels was prepared by embedding them in epoxy resin (EpoFix), followed by mechanical polishing with sandpaper up to 2400 grit size. The exposed surface area of the samples was defined at ~1.2 mm^2 by 3 M™ Scotchrap™ 50 tape. The platinum/iridium SVET probe, having 20 μm diameter, was platinized in a solution containing 10 % (wt/wt) platinum chloride and 1 % (wt/wt) lead (II) acetate to enhance the tip capacitance. Subsequently, using a 15 mM NaCl solution with a 604 Ω cm electrical resistivity, the SVET calibration was performed under the instruction manual of the instrument. The vibration amplitude, vibration frequency, and vibrating electrode distance from the sample were 40 μm, 80 Hz, and 150 μm, respectively. At least two SVET measurements of each kind with 31 × 31 grid points were carried out to ensure the reliability of the results.

To test the antifouling properties, four sets of untreated and treated (PEO and PEO + Cu) samples were immersed in triplicate in a tank with circulating seawater at the Hydrobiological Station Umberto D'Ancona in Chioggia (University of Padua). The biological colonization of the sample surfaces was evaluated after 7, 14, 21, and 28 days of immersion, collecting one set of samples every time. In detail, after the collection, one replicate of each treatment was used to evaluate the antifouling properties through the visual observation at the stereomicroscope Zeiss Stemi 2000-C stereomicroscope (Carl Zeiss, Jena, Germany). Another replicate for the qualitative and quantitative evaluation of the microphytobenthos community was scraped from the treated surface (1 cm^2) of each condition and the fouling was suspended in filtered seawater with 4 % formalin, neutralized with hexamethylenetetramine. The analyses were carried out through an inverted Leitz Diavert microscope (Leitz, Stuttgart, Germany), equipped with the phase contrast, according to the Utermöhl method (1958), observing two transects, equal to the diameter of the sedimentation chamber and with a width corresponding to the diameter of the field of view, with a magnification of 400 X, and reported as cells/cm^2. Microalgal identification was carried out by standard keys, in particular, Peragallo and Peragallo [37], Hustedt [38], Van der Werff & Hulls [39] and Guiry & Guiry [40] were used as

references for diatoms.

3. Results and discussion

3.1. Microstructural characterization

The PEO and PEO + Cu samples were analyzed at the SEM both on the surface and the cross-section, and the results can be found in Fig. 1.

From the observation of the surfaces (Fig. 1A and C), the typical microstructure of these coatings can be noted, with a surface rich in pores, pancake structures, and microcracks. These microstructural features are visible both in the PEO and PEO + Cu samples, and their formations can be linked with the discharge phenomena that typically occur during the PEO process [41]. On the surface of the PEO + Cu sample (Fig. 1C) the presence of copper particles can also be clearly noted, as white spots trapped in the pores (highlighted from the red circles in the photo). The incorporation of particles in the coating occurs, as stated by O'Hara et al. [42], with the main mechanism of incorporation which is the sweeping of suspended particulates into active discharge sites immediately after plasma collapse. Considering the cross-section of the samples (Fig. 1B and D) the presence of the ZA layer (light grey) and the PEO layer (the more external one) can be distinguished. In both the samples (PEO and PEO + Cu) the resulting PEO layer is porous and adherent with the ZA layer, with an average thickness of about 10 μm. Considering the PEO + Cu sample (Fig. 1D) the presence of the copper particles can clearly be noted, trapped in the pores of the PEO layer, which is highlighted by the red circle in the SEM micrograph. A general increase in the porosity of the coating in the PEO + Cu sample in comparison to the PEO sample can also be observed from the analysis of the sample's surface. This fact can be connected with the presence of copper particles in the electrolyte that modify the discharge phenomena producing stronger discharges and causing the formation of bigger pores in the coating [43]. These pores are however present only in the external part of the coating, in fact from the cross-sectional observation higher porosity of the PEO sample in comparison to the PEO + Cu sample can be observed. In detail from the cross-sectional analysis can be found that the coating produced on the PEO + Cu sample is denser but weaker at the interface with the Al—Zn layer. Higher magnification micrograph of the cross section of the sample PEO + Cu can be found reported in Fig. 2. It can be noted as the copper particles are present both in the external part of the coating and in the inner part. The particles that can be found in the inner part are probably trapped into closed discharge channels.

Furthermore, phase analysis was performed on the two coated samples and the results are reported in Fig. 3. As can be noted, besides the presence of the reflections from the substrate (Al and Zn from the Zinc-Aluminized layer) and of the aluminum oxide (coming from the oxidation of the ZA layer) there is the presence of mixed alumina-silicates coming from the interactions between the electrolyte and the substrate. The presence of these mixed compounds is typical of PEO layers and derived from the extremely rapid melting and re-solidification process that occurs through the production of the micro-discharges that are the key to the process [11]. In both the samples,

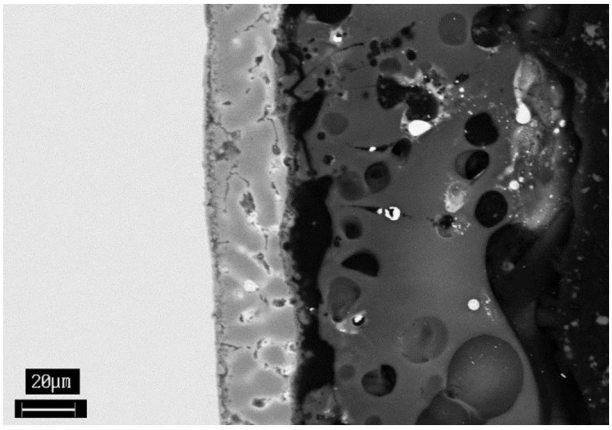

Fig. 2. SEM image of the cross section of the PEO + Cu. The image is recorded in backscattered electron mode.

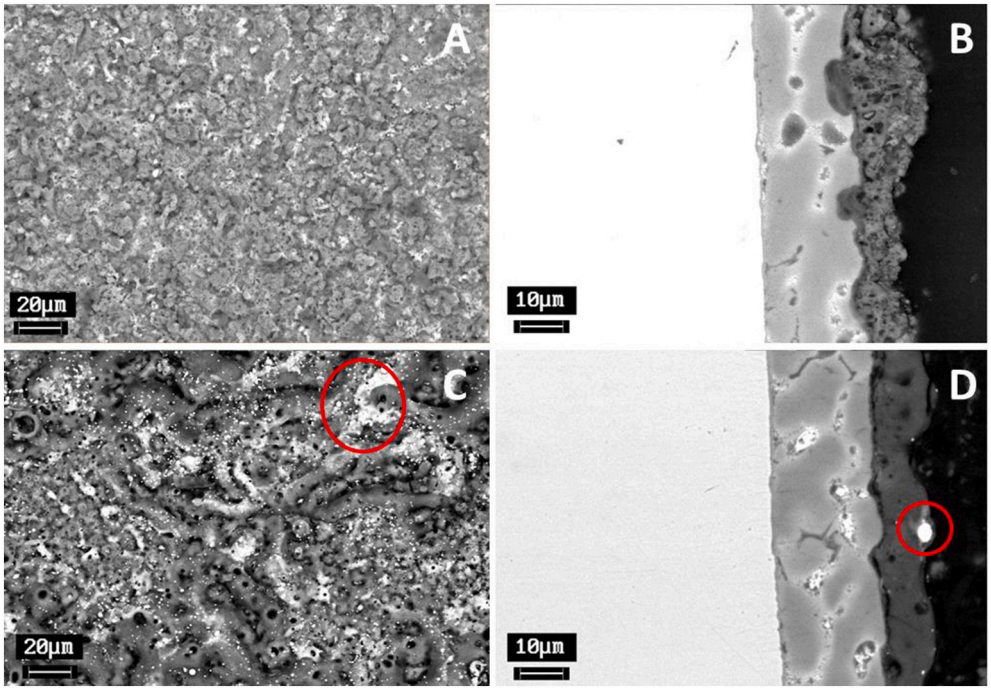

Fig. 1. SEM images of the surface of the PEO treated sample (A) and of the PEO + Cu sample (C) and SEM images of the cross-section of the PEO treated sample (B) and the PEO + Cu sample (D). All the images are recorded in backscattered electron mode and the red circles highlight the presence of the copper particles in the PEO + Cu sample.

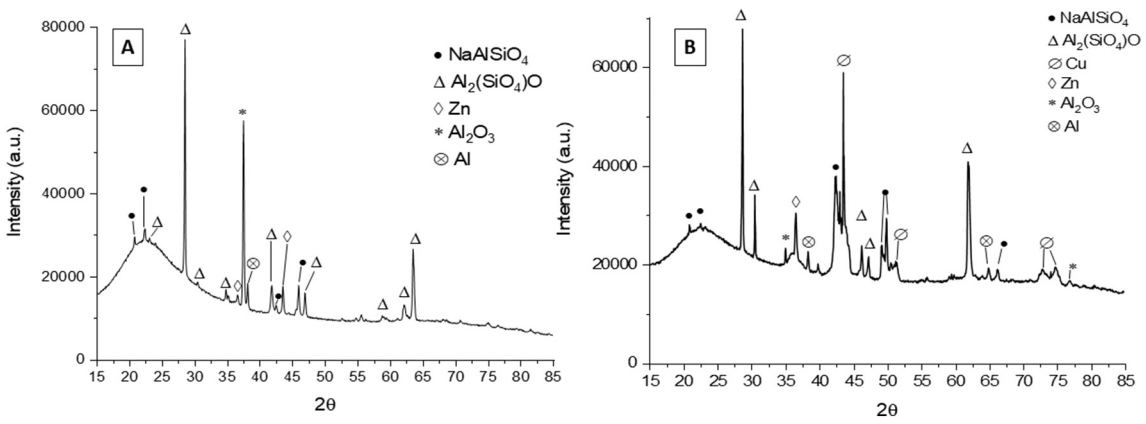

Fig. 3. XRD spectra of the PEO treated sample (A) and the PEO + Cu sample (B).

the presence of a high amorphous fraction into the coating can also be observed. Indeed, this fact is characteristic of the PEO coating [44] and is generally considered the point that is at the base of the improved wear and mechanical properties of PEO coatings in comparison with the ones obtained with traditional anodizing. The main difference in the two reported diffraction patterns resulted the fact that in the sample PEO + Cu (Fig. 3B) are clearly visible the peaks relative to Copper (Cu) that are instead not present in the sample PEO (Fig. 3A), thus confirming the successful incorporation of the particles into the coatings.

3.2. Evaluation of corrosion properties

In order to investigate the corrosion properties of the obtained samples, EIS tests were performed and the results are presented in the form of Nyquist and Bode plots where dots represent experimental data and dashes the result of the fitting. These are reported in Fig. 4. EIS results were also fitted with the equivalent circuit, shown in Fig. 4D, with *Z*-view software. The choice of the circuit was performed according to the literature, and, in particular, with circuits employed for PEO

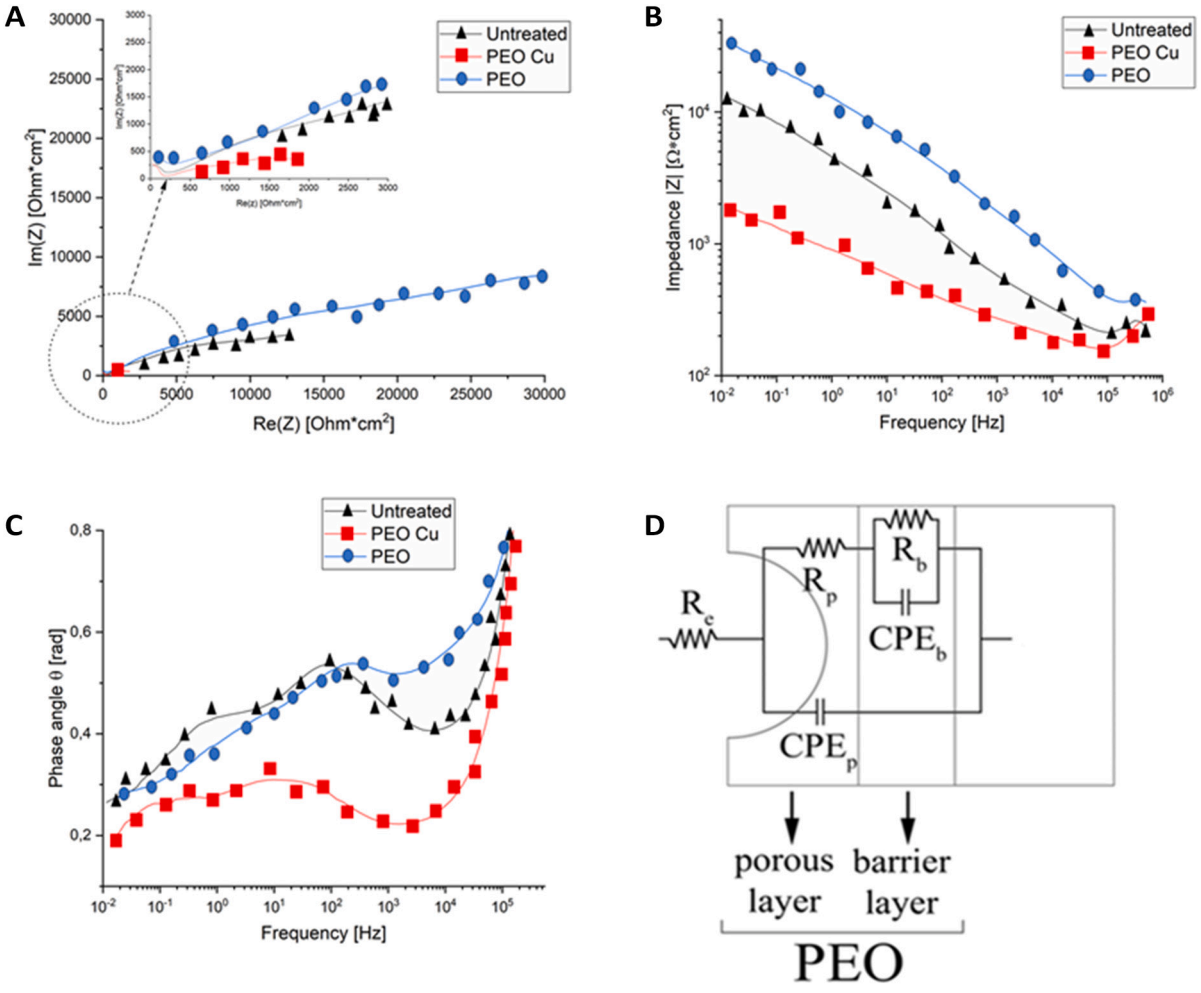

Fig. 4. Results of the EIS tests in the form of a Nyquist Plot (A), Bode Modulus plot (B), and Bode Phase plot (C) for the different samples and equivalent circuits employed for the fitting of the experimental data (D). Test Electrolyte: 0.1 M Na_2SO_4 and 0.05 M NaCl.

coatings [45]. Moreover, the choice was also made on the basis of the shape of the Nyquist and Bode Plots that confirm the presence of two time constants in the PEO-treated samples, requiring the use of two R-CPE in parallel to fit the data. The ZA layer under the PEO coating was not considered in the equivalent circuit, since this layer, for its conductive nature, acts with the substrate as one unique electrochemical unit, under the PEO layer and due to the fact that the penetration of the electrolyte does not reach the steel substrate. The results of the fitting of the experimental data are reported in Table 1 and the low values of chi-squared, together with the good accordance between the dots and the dashes in Fig. 3, demonstrate the good fit. Considering the physical meaning of the different elements of the equivalent circuit in Fig. 4D, R_e represents the resistance of the electrolyte, R_p and CPE_p denote the porous layer of PEO coating, whereas R_b and CPE_b are the barrier layer. PEO layers are, in fact, generally considered composed of two different sub-layers: one inner layer, also called the barrier layer, which gives the main protection against corrosion, and one external porous layer which can be employed to functionalize the surface. CPE_i were used in the equivalent circuits instead of capacitances due to the fact that the measured capacitance is not ideal. In the case of the untreated sample, a single circuit, corresponding to only the barrier layer, was employed in order to consider only the presence of the natural oxide layer.

A first qualitative consideration can be performed by analyzing the Nyquist plot and the Bode Modulus plot, and, in particular, considering the real part of the impedance at the low frequencies (intercept of the semi-circle with the X axis in the case of the Nyquist plot, intercept with the Y axis in the case of the Bode Modulus Plot). This value can be considered a qualitative evaluation of the polarization resistance and, consequently, of the corrosion properties. It can be clearly observed from both the Nyquist and Bode plots that the PEO sample is the one characterized by the higher value of polarization resistance and, therefore, by the higher value of corrosion resistance. Instead, the PEO + Cu sample has the lower polarization resistance, as can be noted in the zoom reported in the top left of the image in Fig. 4A.

Considering the results of the fitting of the experimental data (Table 1), it can be clearly observed that the main differences in the polarization resistance can be ascribed to the barrier layer, and that the resistance R_B of the PEO sample (37,250 Ω) is almost double that of the untreated sample (15,000 Ω) and is one order of magnitude higher than the one of the PEO + Cu sample (1752 Ω). The great differences between the PEO and PEO + Cu samples can be related to the presence of the copper particles. These particles can act as cathodic particles creating galvanic coupling with the substrate (Al—Zn layer) which becomes anodic. This fact can occur when the electrolyte enters the pores that characterize the external layer and can significantly reduce the corrosion properties of the barrier layer, as reported in Table 1. From the results of the fitting, no significant differences in the resistance of the porous layer can be observed, thus confirming the fact that the differences in the corrosion properties are related to the galvanic contact between the copper and the substrate that occur at the interface with the barrier layer, not influencing the properties of the porous layer. Focusing on the values of Q obtained by the fitting and reported in Table 1, these can be considered as more related to the capacitance of the coatings, due to the values of n being higher than 0.8. Considering the values of Q as capacitance, these can be linked with the thickness of the coating, and a smaller value of Q indicates a reduction in the thickness of the coating due to the fact that the capacitance is inversely proportional to the distance between the plates. The value of Q is one order of magnitude higher in the untreated sample in comparison with the PEO-treated samples due to the fact that in the untreated sample only the natural oxide layer, which is thinner than the PEO layer, is formed. Instead, the resulting values of Q were quite similar between the different PEO-treated samples, thus indicating that the thickness of the coating is similar between the various PEO treatments, as also evidenced by the SEM observations reported in Fig. 1. Only a slight increase (less than one order of magnitude) in the value of Q of both the porous and the barrier layer can be noted in the PEO + Cu sample in comparison to the PEO sample. This can probably be linked with an increase in the porosity of the coating in the PEO + Cu sample, already observed with the SEM images of the surfaces and linked with the modification in the discharge phenomena due to the presence of the copper particles, which produce an increase in the penetration of the electrolyte into the coating and so an increase in the capacitance value. In fact, the lower capacitance values at the coating interface indicate the lower electrolyte penetration because the electrolyte has a higher dielectric constant value than the oxide coating. [45] The differences in the corrosion behavior observed between the PEO and the PEO + Cu samples can be also related to the different interface formed in the two cases. In detail from the previously reported SEM observation the interface resulted weaker in the PEO + Cu samples, thus producing a decrease in the corrosion properties due to the fact that the electrolyte can penetrate more easily between the ZA layer and the PEO coating due to the presence of a very weak interface. This fact is also confirmed by the slight increase in the capacitances values in the PEO + Cu sample. Considering that the variations in the corrosion behavior of the PEO and PEO + Cu samples were mainly related to the presence of the copper particles, it could be very interesting to study the electrochemical behavior of the coating near the particles in more depth, in order to better study the corrosion mechanism in the PEO + Cu samples. For this reason, localized corrosion tests (SVET tests) were also performed.

The corrosion behavior of the coupons was investigated through the SVET test after up to 12 h immersion in 0.015 M NaCl electrolyte (Fig. 5). The cut-edge design was employed to obtain the SVET findings in a way that the exposed area of the coated samples was 1.2 mm^2 (shown as a black rectangle on the maps). For the untreated sample, the sacrificial role of the commercial Galvalume was noticed at the borders of the exposed area ($j > 0$), while cathodic reactions took place over the carbon steel ($j < 0$). The carbon steel was protected whereas the Galvalume coating was selectively dissolved in the chloride electrolyte [46]. Moreover, A. Pritzel dos Santos et al. reported the ability of the Galvalume to protect the substrate in the cut-edge set-up [47]. For the PEO sample, the same behavior was observed in which the cathodic activities occurred at the center and local anodic activity at the border. The anodic peak intensity of the PEO was lower than untreated samples, which is in a good agreement with EIS and PDP investigations. It is worthwhile mentioning that the difference in anodic peak intensity is not necessarily indicative of different rates of corrosion, as the local corrosion activities are time-dependent and the scanning probe is prone to lose some data during point-by-point scanning [31]. The corrosion behavior of the PEO + Cu was initiated at the borders, like the untreated and PEO samples. But, after a while, the anodic activity spots extended at the exposed area, illustrating the progressive galvanic corrosion happening between the substrate and copper. The addition of copper into the PEO coating not only enhanced the anodic regions but also the anodic intensity (j values). Optical images were taken at the end of the immersion test, confirming the adverse impact of the copper added to

Table 1
Results of the fitting of the experimental data coming from EIS tests using the circuit reported in Fig. 4.

Sample	R_e [Ωcm^2]	R_B [Ωcm^2]	R_p [Ωcm^2]	Q_p [Fcm^{-2}Hz^{1-n}]	n_p	Q_B [Fcm^{-2}Hz^{1-n}]	n_B	X^2
Untreated	80	15,000	–	–	–	2.55*10^{-6}	0.85	0.0002
PEO Cu	74	1752	365	7.75*10^{-5}	0.84	7.00*10^{-7}	0.89	0.0006
PEO	76	37,250	548	3.12*10^{-5}	0.83	2.00*10^{-7}	0.83	0.0004

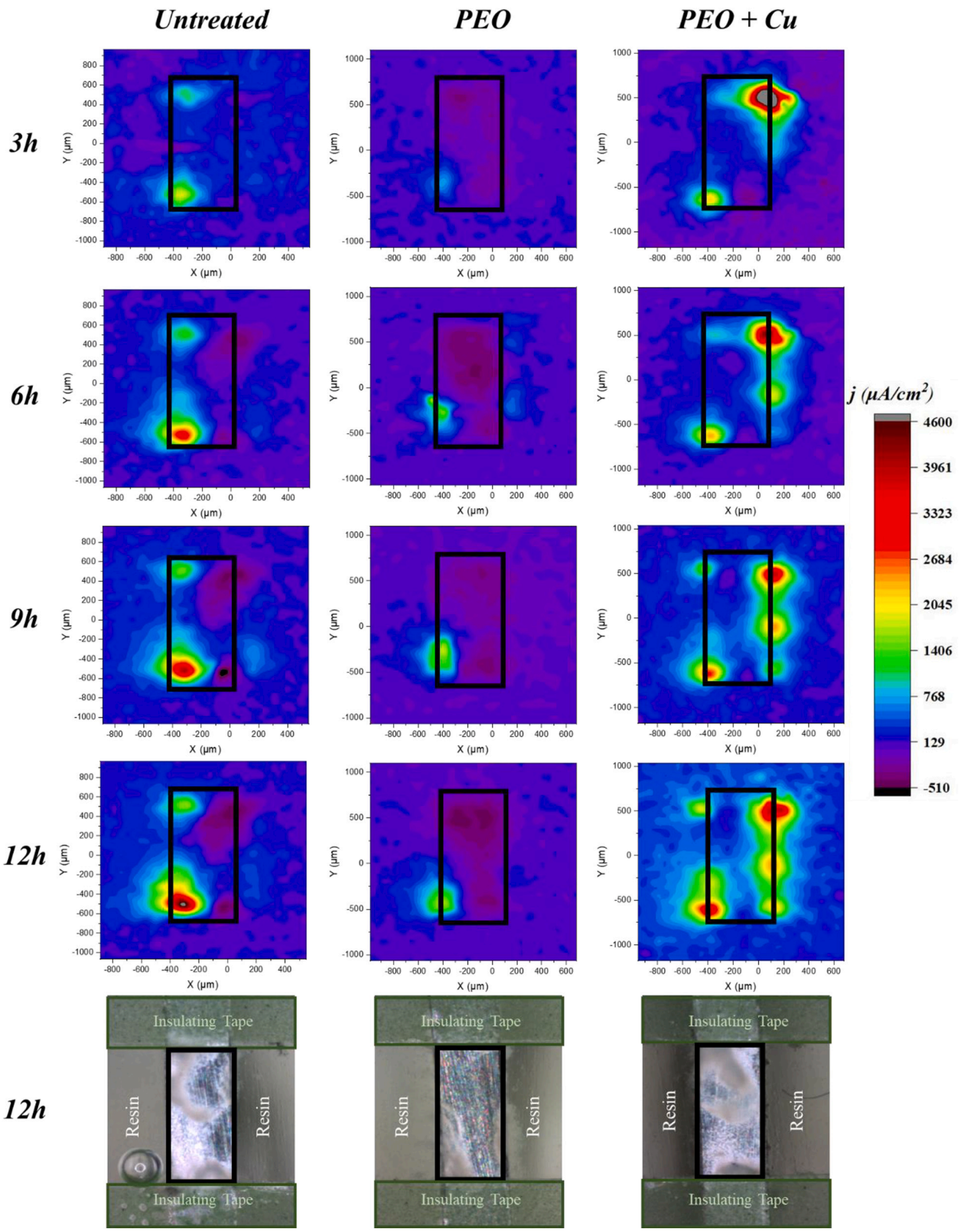

Fig. 5. SVET maps of untreated, PEO, and PEO + Cu samples during 12 h immersion in 15 mM NaCl electrolyte. The optical image was taken at the end of the immersion test (12*h*), illustrating the exposed area with a black rectangle.

the PEO coating on corrosion protection performance. Therefore, the order of the samples, in terms of the corrosion protection properties, is PEO > substrate>PEO + Cu.

3.3. *Evaluation of antifouling properties*

To evaluate the antifouling properties, one replicate of the samples was firstly analyzed with photographic and stereomicroscope

observations, and these results can be found in Fig. 6 for 0, 7, and 14 days of immersion, and in Fig. 7 for 21 and 28 days of immersion. In the photographic observation can be observed the whole sample but the PEO treated zone is only the lower one (1cm^2). The stereo-microscope observation was performed only in the PEO treated area. The observation at 0 day of immersion (Fig. 6) allowed the samples to be considered before the immersion in seawater: the typical light grey color of the PEO coating can clearly be noted, whereas the presence of the copper particles gives the sample a brown appearance. After 7 days of immersion (Fig. 6) colonization forms cannot be seen on any of the samples. Only on the PEO + Cu sample is there the appearance of white zones that can be related to the start of corrosion phenomena. As previously explained, this sample is the one characterized by the lower corrosion properties, and the oxides of Zinc and Aluminum, which constitute the layer, are generally white. After 14 days of immersion (Fig. 6), using the stereo microscope observation, the start of colonization phenomena can clearly be observed in the untreated and PEO-treated samples. No colonization

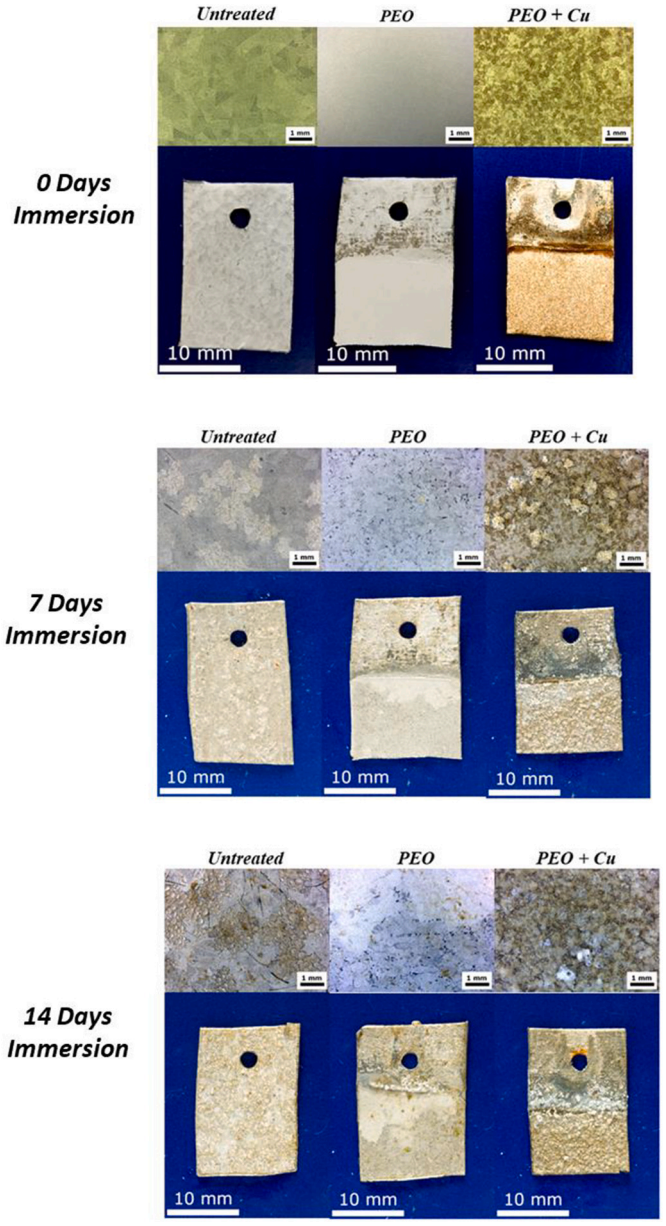

Fig. 6. Results of the antifouling tests in circulating seawater. Photographic and stereo-microscope observation of the samples before the immersion and after 7 and 14 days of immersion.

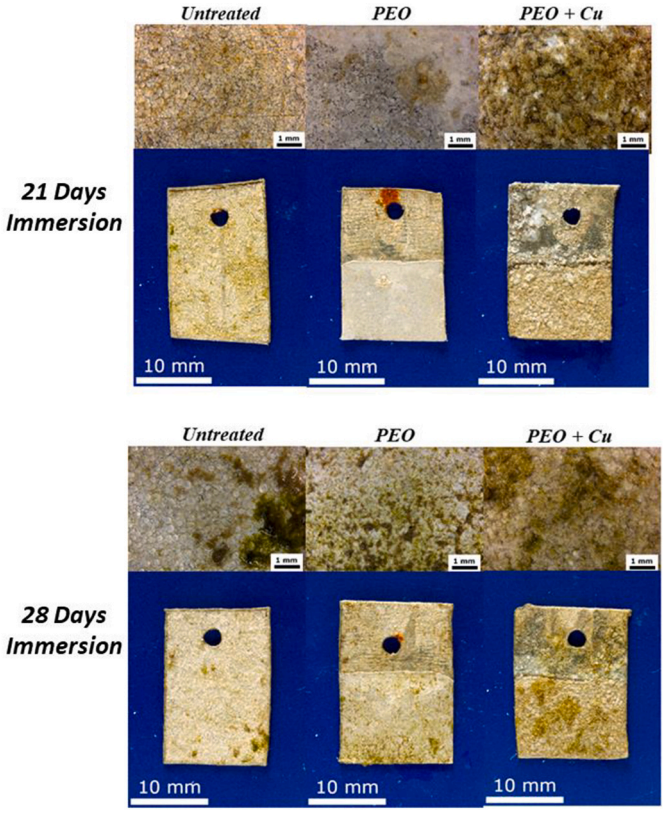

Fig. 7. Results of the antifouling tests in circulating seawater. Photographic and stereomicroscope observation of the samples after 21 and 28 days of immersion.

can be noted in the PEO + Cu sample, where the corrosion phenomena is observable through the formation of the white corrosion products. This fact can be related to the antifouling properties of the copper particles that do not permit the colonization phenomena to start after 14 days of immersion. This behavior was confirmed after 21 days of immersion (Fig. 7). Indeed, in this case, colonization was remarkably reduced in the PEO + Cu sample in comparison to the untreated sample, which was completely colonized, and the PEO-treated sample had diffused colonized zones. Also, after 21 days of immersion, the presence of white corrosion products were instead visible on the PEO + Cu sample and not on the PEO sample. After 28 days of immersion (Fig. 7) the colonization also seemed to start on the PEO + Cu sample, probably due to the fact that the complete coverage of the surface of the samples by the biofilm significantly reduced the antifouling effect of the copper particles present in the PEO underlayer. Furthermore, the corrosion products seemed to be covered by the fouling.

Cross section of the sample PEO + Cu after 28 days of immersion was also analyzed at the SEM and the results are reported in Fig. 8. As can be clearly noted the corrosion produce the detachment of part of the PEO layer, as can be partially expected due to the weak interface previously observed in the sample PEO + Cu. As can be partially observed in Fig. 8A and more clearly noted in Fig. 8B (highlighted by the red circles) the corrosion has penetrated the PEO layer and have clearly attacked also the ZA layer without arriving to the steel substrate.

3.4. Biological analyses

Observations using the light microscope on the different samples (untreated, PEO + Cu, and PEO) showed an almost complete presence of photosynthetic species, belonging to the group Bacillariophyceae (phylum Heterokontophyta). However, some filamentous Cyanophyta and Chlorophyta were observed on some samples. The prevalence of

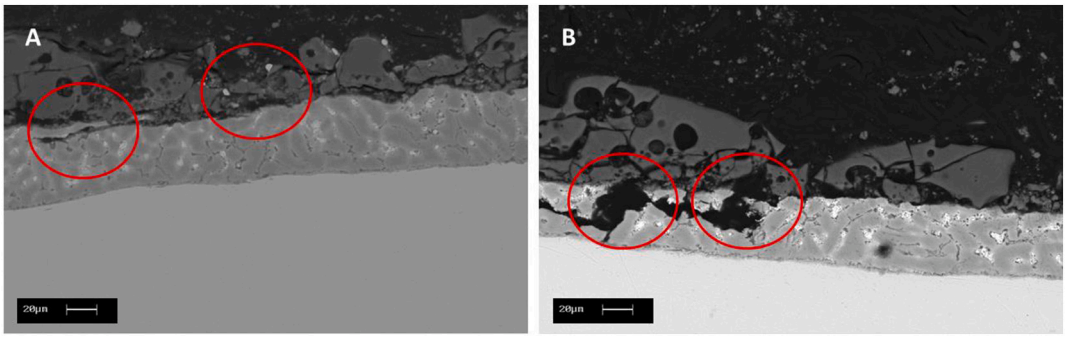

Fig. 8. Cross sectional SEM micrographs of the PEO + Cu sample after 28 days of immersion.

diatom cells, already observed in other research carried out on PEO-coated samples by Cerchier et al., confirms the dominance of this group of microalgae in the microphytobenthos communities. Among the diatoms, there was the almost complete presence of pennate diatoms, a group of microalgae represented mainly by benthic taxa. These microalgae are able to attach to the substrates through their valves (adnate diatoms) or stalks (erect diatoms) [48].

During the first week of immersion in seawater, qualitative analyses showed the presence of 31 diatom taxa in the untreated sample, while in the PEO + Cu had 5 and the PEO 25. Quantitative analyses highlighted a cell density of 6680 cells/cm^2 in the untreated sample, while in the PEO + Cu and PEO samples, the total cell densities were 1040 and 5920 cells/cm^2, respectively (Fig. 9).

After 14 days of immersion, the number of taxa decreased in the untreated sample, while it increased in the PEO + Cu and PEO samples, reaching a number of 8 and 39 taxa, respectively. It is evident that the PEO sample was characterized by a higher number of taxa, and among them, there was the presence of both adnate and erect species. Quantitative analyses showed a cell density of 7120 cells/cm^2 in the untreated sample, while in the PEO + Cu and PEO samples, the total cell densities were 1960 and 31,120 cells/cm^2, respectively (Fig. 9). These high cell density values were due to the high cell number of the species *Halamphora veneta*, *Tryblionella acuminata*, *Thalassionema nitzschioides* and undetermined pennate taxa.

The highest number of taxa registered after 21 days of immersion was in the PEO sample, with 35 taxa. In the untreated and PEO + Cu samples, the number of taxa was 27 and 12, respectively. Among the samples collected after the third week (21 days of immersion), both in the untreated and PEO samples, the most common taxa were erect forms, such as *Licmophora flabellata* (Fig. 10A), a diatom forming great fan-shaped colonies attached to the substrates thanks to the presence of stalks. In the PEO + Cu samples, the most frequent forms were epontic taxa, which are loosely-attached species, sometimes described as "plocon" diatoms [49]. Results regarding the quantitative analyses highlighted the highest total cell density values in the PEO sample, reaching a cell density of 192,160 cells/cm^2, followed by the value of 146,000 cells/cm^2 in the untreated sample and 16,000 cells/cm^2 in the PEO + Cu treatment (Fig. 9).

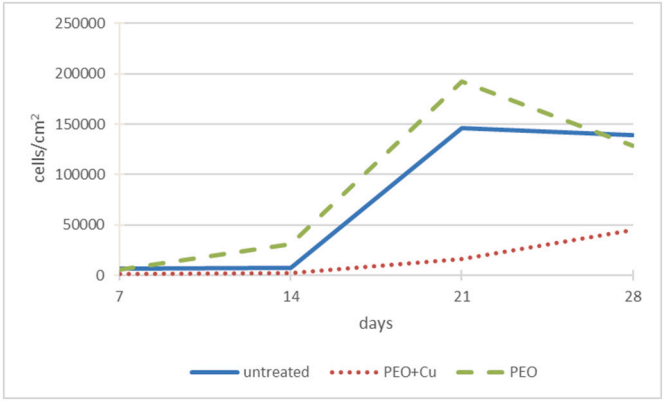

Fig. 9. Total cell density of microalgae counted for the different treatments during the biofouling colonization.

After 28 days of immersion, the number of taxa on the untreated and the PEO samples was nearly constant, while for the PEO + Cu treatment, a slight increase in the number of species was observed. As regards the quantitative data, for the untreated and PEO samples, cell densities lower than the values of 21 days were registered, with 139,720 and 128,640 cells/cm^2, respectively. In the PEO + Cu, the total cell density was 45,120 cells/cm^2 (Fig. 9), a value higher than that registered after 21 days of immersion, but lower than those registered for the other treatments. This high value was mainly due to the presence of plocon species.

In addition to the diatom component, only in the untreated sample after 7 days of immersion and in the PEO samples after 14 and 21 days of immersion, the presence of chlorophycean filaments was also registered (Fig. 10B). In the PEO + Cu, after 28 days of immersion, the presence of few trichomes of *Spirulina* sp. (Cyanophyta) was observed.

The high cell density observed for the PEO treatment showed that this treatment is less efficient in the antifouling process. The PEO treatment increased biofouling colonization, due to the morphology of this specific coating. These results are in agreement with the observations in Cerchier et al. [50], where the PEO sample showed less efficacy as antifouling than PEO + Cu one. Also in this research, the low number of taxa, and the lower cell density registered for the PEO + Cu treatment, revealed that this treatment was the most efficient against colonization by biofouling (Fig. 9).

4. Conclusions

Considering the previously reported results the following main conclusion can be drawn:

- The corrosion properties were strongly influenced by the presence of the copper particles that were detrimental to the corrosion properties of the PEO layer causing galvanic coupling with the zinc-aluminized substrate.
- The copper particles appear to have a strong antifouling effect, inhibiting the colonization phenomena for 21 days of immersion.
- The biofouling data of the PEO + Cu treatment showed a lower number of species and lower cell density than the untreated and PEO-coated samples.
- For longer immersion times, the complete covering of the surface by the biofilm reduces the antifouling effect of the particles.
- Considering the fact that the PEO + Cu treatment confers good antifouling properties to the steel, as well as a decrease in the corrosion properties, the treatment can be suggested as a pre-

Fig. 10. Light micrographs of Licmophora flabellata (A) and a chlorophycean filament (B). Scale bar = 10 μm.

treatment, but a top-coat that confers good corrosion properties must be employed for real in-situ applications.

Funding

Project supported by the BIRD 2020 program of the University of Padova (Project BIRD202558/20).

CRediT authorship contribution statement

Luca Pezzato: Writing – review & editing, Writing – original draft, Validation, Investigation, Formal analysis, Data curation, Conceptualization. **Sajjad Akbarzadeh:** Writing – review & editing, Writing – original draft, Investigation, Formal analysis, Data curation. **Alessio Giorgio Settimi:** Validation, Investigation, Formal analysis, Data curation. **Emanuela Moschin:** Visualization, Investigation, Formal analysis, Data curation. **Isabella Moro:** Writing – original draft, Visualization, Formal analysis, Data curation. **Marie-Georges Olivier:** Writing – review & editing, Supervision, Methodology. **Katya Brunelli:** Writing – review & editing, Supervision, Resources, Funding acquisition, Conceptualization. **Manuele Dabalà:** Supervision, Resources, Project administration, Funding acquisition, Conceptualization.

Declaration of competing interest

The authors declare that they have no known competing financial interests or personal relationships that could have appeared to influence the work reported in this paper.

References

[1] L. Pezzato, C. Gennari, M. Franceschi, K. Brunelli, Influence of silicon morphology on direct current plasma electrolytic oxidation process in AlSi10Mg alloy produced with laser powder bed fusion, Sci. Rep. 12 (2022) 1–17, https://doi.org/10.1038/s41598-022-18176-x.

[2] M. Kaseem, B. Dikici, Optimization of surface properties of plasma electrolytic oxidation coating by organic additives: a review, Coatings 11 (2021) 1–23, https://doi.org/10.3390/coatings11040374.

[3] Y. Chen, X. Lu, S.V. Lamaka, P. Ju, C. Blawert, T. Zhang, F. Wang, M. L. Zheludkevich, Active protection of Mg alloy by composite PEO coating loaded with corrosion inhibitors, Appl. Surf. Sci. 504 (2020) 144462, https://doi.org/10.1016/j.apsusc.2019.144462.

[4] M. Molaei, K. Babaei, A. Fattah-alhosseini, Improving the wear resistance of plasma electrolytic oxidation (PEO) coatings applied on Mg and its alloys under the addition of nano- and micro-sized additives into the electrolytes: a review, J. Magnes. Alloy 9 (2021) 1164–1186, https://doi.org/10.1016/j.jma.2020.11.016.

[5] X. Lu, M. Mohedano, C. Blawert, E. Matykina, R. Arrabal, K.U. Kainer, M. L. Zheludkevich, Plasma electrolytic oxidation coatings with particle additions – a review, Surf. Coatings Technol. 307 (2016) 1165–1182, https://doi.org/10.1016/j.surfcoat.2016.08.055.

[6] K. Babaei, A. Fattah-alhosseini, M. Molaei, The effects of carbon-based additives on corrosion and wear properties of plasma electrolytic oxidation (PEO) coatings applied on aluminum and its alloys: a review, Surfaces and Interfaces 21 (2020) 100677, https://doi.org/10.1016/j.surfin.2020.100677.

[7] A. Fattah-alhosseini, M. Molaei, K. Babaei, The effects of nano- and micro-particles on properties of plasma electrolytic oxidation (PEO) coatings applied on titanium substrates: a review, Surfaces and Interfaces 21 (2020) 100659, https://doi.org/10.1016/j.surfin.2020.100659.

[8] S. Akbarzadeh, Y. Paint, M.-G. Olivier, A comparative study of different sol-gel coatings for sealing the plasma electrolytic oxidation (PEO) layer on AA2024 alloy, Electrochim. Acta 443 (2023) 141930, https://doi.org/10.1016/j.electacta.2023.141930.

[9] A.S. Gnedenkov, S.L. Sinebryukhov, V.S. Filonina, S.V. Gnedenkov, Hydroxyapatite-containing PEO-coating design for biodegradable Mg-0.8Ca alloy: formation and corrosion behaviour, J. Magnes. Alloy. (2022), https://doi.org/10.1016/j.jma.2022.12.002.

[10] J.A. Curran, H. Kalkanci, Y. Magurova, T.W. Clyne, Mullite-rich plasma electrolytic oxide coatings for thermal barrier applications, Surf. Coatings Technol. 201 (2007) 8683–8687, https://doi.org/10.1016/j.surfcoat.2006.06.050.

[11] H. Dong, Surface Engineering of Light Alloys Aluminium, Magnesium and Titanium Alloys, 2010.

[12] E. Nikoomanzari, M. Karbasi, W.C.M.A. Melo, H. Moris, K. Babaei, S. Giannakis, A. Fattah-alhosseini, Impressive strides in antibacterial performance amelioration of Ti-based implants via plasma electrolytic oxidation (PEO): a review of the recent advancements, Chem. Eng. J. 441 (2022) 136003, https://doi.org/10.1016/j.cej.2022.136003.

[13] A. Fattah-alhosseini, K. Babaei, M. Molaei, Plasma electrolytic oxidation (PEO) treatment of zinc and its alloys: a review, Surfaces and Interfaces. 18 (2020) 100441, https://doi.org/10.1016/j.surfin.2020.100441.

[14] K. Babaei, A. Fattah-alhosseini, R. Chaharmahali, A review on plasma electrolytic oxidation (PEO) of niobium: mechanism, properties and applications, Surfaces and Interfaces. 21 (2020) 100719, https://doi.org/10.1016/j.surfin.2020.100719.

[15] A. Fattah-alhosseini, R. Chaharmahali, M.K. Keshavarz, K. Babaei, Surface characterization of bioceramic coatings on Zr and its alloys using plasma electrolytic oxidation (PEO): a review, Surfaces and Interfaces 25 (2021) 101283, https://doi.org/10.1016/j.surfin.2021.101283.

[16] Y.L. Wang, M. Wang, M. Zhou, B.J. Li, G. Amoako, Z.H. Jiang, Microstructure characterisation of alumina coating on steel by PEO, Surf. Eng. 29 (2013) 271–275, https://doi.org/10.1179/1743294412Y.0000000084.

[17] Y. Wang, Z. Jiang, Z. Yao, H. Tang, Microstructure and corrosion resistance of ceramic coating on carbon steel prepared by plasma electrolytic oxidation, Surf. Coatings Technol. 204 (2010) 1685–1688, https://doi.org/10.1016/j.surfcoat.2009.10.023.

[18] N. Attarzadeh, M. Molaei, K. Babaei, A. Fattah-alhosseini, New promising ceramic coatings for corrosion and wear protection of steels: a review, Surfaces and Interfaces. 23 (2021) 100997, https://doi.org/10.1016/j.surfin.2021.100997.

[19] S. A., H. S., A. S., R.K. L., R. N, Effect of electrolyte composition on morphology and corrosion resistance of plasma electrolytic oxidation coatings on aluminized steel, Surf. Coatings Technol. 372 (2019) 239–251, https://doi.org/10.1016/j.surfcoat.2019.05.047.

[20] L. Pezzato, A.G. Settimi, P. Cerchier, C. Gennari, M. Dabalà, K. Brunelli, Microstructural and corrosion properties of PEO coated zinc-aluminized (ZA) steel, Coatings 10 (2020) 1–12, https://doi.org/10.3390/COATINGS10050448.

[21] F. Songur, E. Arslan, B. Dikici, Taguchi optimization of PEO process parameters for corrosion protection of AA7075 alloy, Surf. Coatings Technol. 434 (2022) 128202, https://doi.org/10.1016/j.surfcoat.2022.128202.

[22] R.O. Hussein, P. Zhang, X. Nie, Y. Xia, D.O. Northwood, The effect of current mode and discharge type on the corrosion resistance of plasma electrolytic oxidation (PEO) coated magnesium alloy AJ62, Surf. Coatings Technol. 206 (2011) 1990–1997, https://doi.org/10.1016/j.surfcoat.2011.08.060.

[23] A. Hakimizad, K. Raeissi, M. Santamaria, M. Asghari, Effects of pulse current mode on plasma electrolytic oxidation of 7075 Al in Na2WO4 containing solution: from unipolar to soft-sparking regime, Electrochim. Acta 284 (2018) 618–629, https://doi.org/10.1016/j.electacta.2018.07.200.

[24] A.B. Rogov, A. Nemcova, T. Hashimoto, A. Matthews, A. Yerokhin, Analysis of electrical response, gas evolution and coating morphology during transition to soft

sparking PEO of Al, Surf. Coatings Technol. 442 (2022) 128142, https://doi.org/10.1016/j.surfcoat.2022.128142.
[25] D.S. Tsai, C.C. Chou, Review of the soft sparking issues in plasma electrolytic oxidation, Metals (Basel) 8 (2018) 1–22, https://doi.org/10.3390/met8020105.
[26] T.W. Clyne, S.C. Troughton, A review of recent work on discharge characteristics during plasma electrolytic oxidation of various metals, Int. Mater. Rev. 64 (2019) 127–162, https://doi.org/10.1080/09506608.2018.1466492.
[27] A. Fattah-alhosseini, R. Chaharmahali, K. Babaei, Effect of particles addition to solution of plasma electrolytic oxidation (PEO) on the properties of PEO coatings formed on magnesium and its alloys: a review, J. Magnes. Alloy 8 (2020) 799–818, https://doi.org/10.1016/j.jma.2020.05.001.
[28] X. Lu, C. Blawert, K.U. Kainer, T. Zhang, F. Wang, M.L. Zheludkevich, Influence of particle additions on corrosion and wear resistance of plasma electrolytic oxidation coatings on Mg alloy, Surf. Coatings Technol. 352 (2018) 1–14, https://doi.org/10.1016/j.surfcoat.2018.08.003.
[29] S. Stojadinović, N. Radić, R. Vasilić, High photocatalytic activity of TiO2/Al2TiO5 coatings obtained by plasma electrolytic oxidation of titanium, Mater. Lett. 338 (2023), https://doi.org/10.1016/j.matlet.2023.134069.
[30] L. Pezzato, P. Cerchier, K. Brunelli, A. Bartolozzi, R. Bertani, M. Dabalà, Plasma electrolytic oxidation coatings with fungicidal properties*, Surf. Eng. 35 (2019) 325–333, https://doi.org/10.1080/02670844.2018.1441659.
[31] P. Cerchier, L. Pezzato, E. Moschin, L.B. Coelho, M.G.M. Olivier, I. Moro, M. Magrini, Antifouling properties of different plasma electrolytic oxidation coatings on 7075 aluminium alloy, Int. Biodeterior. Biodegrad. 133 (2018) 70–78, https://doi.org/10.1016/j.ibiod.2018.06.005.
[32] L. Pezzato, A.G. Settimi, D. Fanchin, E. Moschin, I. Moro, M. Dabalà, Effect of Cu addition on the corrosion and antifouling properties of PEO coated zinc-aluminized steel, Materials (Basel) 15 (2022) 7895, https://doi.org/10.3390/ma15227895.
[33] K.A. Dafforn, J.A. Lewis, E.L. Johnston, Antifouling strategies: history and regulation, ecological impacts and mitigation, Mar. Pollut. Bull. 62 (2011) 453–465, https://doi.org/10.1016/j.marpolbul.2011.01.012.
[34] M. Pérez, M. García, G. Blustein, Evaluation of low copper content antifouling paints containing natural phenolic compounds as bioactive additives, Mar. Environ. Res. 109 (2015) 177–184, https://doi.org/10.1016/j.marenvres.2015.07.006.
[35] P.M. Ashraf, L. Edwin, Nano copper oxide incorporated polyethylene glycol hydrogel: an efficient antifouling coating for cage fishing net, Int. Biodeterior. Biodegrad. 115 (2016) 39–48, https://doi.org/10.1016/j.ibiod.2016.07.015.
[36] L. Braithwaite, K. Albrechtas, D. Zagidulin, M. Behazin, D. Shoesmith, J.J. Noël, Galvanic coupling of copper and carbon steel in the presence of bentonite clay and chloride, J. Electrochem. Soc. 169 (2022) 051502, https://doi.org/10.1149/1945-7111/ac5ff2.
[37] H. Peragallo, M. Peragallo, Diatomees Marine de France et des Districts Maritimes Voisins, Micrographe Editeur Grez sur Loing (S. et M.), n.d.
[38] F. Husted, Die Kiesealgen Von Deutschland, Österreichs Und der Schweiz Mit Berusichtigung der Übrigen Länder Europas Sowie der Angrenzender Mehresgebiete., in: Rabenhorst's Kriptogamen-Flora Von Deutschland, Österreichs Und Der Schweiz, Akad, M.B.H, Verlag., Leipzig, n.d.
[39] A. Van der Werff, H. Hulls, Diatomeeën flora Van Nederland., Science Publishers, Koeningstein, n.d.
[40] M.D. Guiry, G.M. Guiry, AlgaeBase, World-wide electronic publication, 2023. https://www.algaebase.org.
[41] R.O. Hussein, X. Nie, D.O. Northwood, An investigation of ceramic coating growth mechanisms in plasma electrolytic oxidation (PEO) processing, Electrochim. Acta 112 (2013) 111–119, https://doi.org/10.1016/j.electacta.2013.08.137.
[42] M. O'Hara, S.C. Troughton, R. Francis, T.W. Clyne, The incorporation of particles suspended in the electrolyte into plasma electrolytic oxidation coatings on Ti and Al substrates, Surf. Coatings Technol. 385 (2020) 125354, https://doi.org/10.1016/j.surfcoat.2020.125354.
[43] S.C. Troughton, A. Nominé, J. Dean, T.W. Clyne, Effect of individual discharge cascades on the microstructure of plasma electrolytic oxidation coatings, Appl. Surf. Sci. 389 (2016) 260–269, https://doi.org/10.1016/j.apsusc.2016.07.106.
[44] A.M. Pillai, R. Ghosh, A. Dey, K. Prajwal, A. Rajendra, A.K. Sharma, S. Sampath, Crystalline and amorphous PEO based ceramic coatings on AA6061: Nanoindentation and corrosion studies, Ceram. Int. 47 (2021) 14707–14716, https://doi.org/10.1016/j.ceramint.2021.01.147.
[45] V.S. Dilimon, S.M.A. Shibli, A review on the application-focused assessment of plasma electrolytic oxidation (PEO) coatings using electrochemical impedance spectroscopy, Adv. Eng. Mater. 25 (2023) 1–18, https://doi.org/10.1002/adem.202201796.
[46] H.N. McMurray, Localized corrosion behavior in aluminum-zinc alloy coatings investigated using the scanning reference electrode technique, Corrosion 57 (2001) 313–322, https://doi.org/10.5006/1.3290355.
[47] A. Pritzel dos Santos, S.M. Manhabosco, J.S. Rodrigues, L.F.P. Dick, Comparative study of the corrosion behavior of galvanized, galvannealed and Zn55Al coated interstitial free steels, Surf. Coatings Technol. 279 (2015) 150–160, https://doi.org/10.1016/j.surfcoat.2015.08.046.
[48] F.E. Round, R.M. Crawford, D.G. Mann, The Diatoms. Biology and Morphology of the Genera, Cambridge University Press, Cambridge UK, 1990.
[49] F.E. Round, The Ecology of Algae, Cambridge University Press, Cambridge UK, 1981.
[50] P. Cerchier, L. Pezzato, C. Gennari, E. Moschin, I. Moro, M. Dabalà, PEO coating containing copper: a promising anticorrosive and antifouling coating for seawater application of AA 7075, Surf. Coatings Technol. 393 (2020) 125774, https://doi.org/10.1016/j.surfcoat.2020.125774.